Semimicroscopic analysis of ^{6}Li + ^{28}Si elastic scattering at 76 to 318 MeV

M. A. Hassanain,[1,2] M. Anwar,[3] and Kassem O. Behairy[3]
[1]*Department of Physics, King Khalid University, Abha, Saudia Arabia*
[2]*Department of Physics, New-Valley Faculty of Science, Assiut University, El-Kharga, Egypt*
[3]*Department of Physics, Faculty of Science, Aswan University, Aswan, Egypt*

(Received 27 October 2017; revised manuscript received 4 March 2018; published 18 April 2018)

Using the α-cluster structure of colliding nuclei, the elastic scattering of ^{6}Li + ^{28}Si at energies from 76 to 318 MeV has been investigated by the use of the real folding cluster approach. The results of the cluster analysis are compared with those obtained by the CDM3Y6 effective density- and energy-dependent nucleon-nucleon (*NN*) interaction based upon *G*-matrix elements of the M3Y-Paris potential. A Woods-Saxon (WS) form was used for the imaginary potential. For all energies and derived potentials, the diffraction region was well reproduced, except at $E_{\rm lab} = 135$ and 154 MeV at large angle. These results suggest that the addition of the surface (DWS) imaginary potential term to the volume imaginary potential is essential for a correct description of the refractive structure of the ^{6}Li elastic scattering distribution at these energies. The energy dependence of the total reaction cross sections and that of the real and imaginary volume integrals is also discussed.

DOI: 10.1103/PhysRevC.97.044610

I. INTRODUCTION

The investigations of elastic scattering differential cross sections of nucleons and composite projectiles from nuclei are of great interest to determine the projectile-nucleus interaction potential. Particularly, ^{6}Li elastic scattering is of considerable interest, not only because of the pronounced failure of the microscopic model to predict its data, as pointed by Satchler and Love [1], but also due to the intermediate position of ^{6}Li ions in the mass range of $A = 4$–12 ions, whose elastic scatterings exhibit a transition between that characteristic of light ions ($A \leqslant 4$) and that characteristic of heavy ions (HIs) ($A \geqslant 12$) [1]. Therefore, such data could provide an essential test for the validity of any model for HI potentials [2–5].

The optical model (OM) analysis of HI scattering data is usually performed by the use of the double-folding (DF) potential as well as the phenomenological description. The DF procedure is limited to the real part of the optical potential while the imaginary potential is fitted in a phenomenological form.

Microscopically, ^{6}Li has presented a problem in the DF model description, where the real potential required a normalization of approximately one-half in order to reproduce the data. Branden *et al.* [6] assumed that this is due to the importance of breakup channels for the loosely bound ^{6}Li nucleus. This effect is represented by a complex dynamical polarization potential (DPP) which has a strongly repulsive real part. Several theoretical calculations [7–9], including continuum discretized coupled channel (CDCC) calculations, showed that the renormalization factor is close to unity when the coupling to breakup channels is included.

During the 1970s to 1980s [1,10–15], ^{6}Li elastic scattering from various targets was extensively studied with bombarding energies below 200 MeV. Nadasen *et al.* from 1988 to 1993 reported a series of systematic studies [16–18] of ^{6}Li scattering off ^{12}C, ^{28}Si, ^{40}Ca, ^{58}Ni, ^{90}Zr, and ^{208}Pb at 210 MeV and from ^{12}C and ^{28}Si at 318 MeV with phenomenological and folding-model potentials. A study of ^{6}Li scattering on ^{12}C, ^{58}Ni, ^{90}Zr, and ^{208}Pb targets at 600 MeV [19] was reported in 2000, investigating the coupling effect between the elastic and the breakup channels at intermediate energies, and these data were successfully fitted in 2014 [20]. Finally, between 2007 and 2010 [21–23], 240 MeV ^{6}Li elastic and inelastic scattering on ^{116}Sn, ^{24}Mg, ^{28}Si, ^{58}Ni, ^{90}Zr, ^{40}Ca, and ^{48}Ca was carried out by Chen and his group. They used the optical potential model to fit the data, where the DF model was used to construct the real part and a Woods-Saxon (WS) shape represented the imaginary part. Alternatively, another theoretical method was used to calculate the real part of the nucleus-nucleus potential using the energy-density functional (EDF) theory from the difference in the total energies of the two interacting nuclei at finite and infinite separation. The real part of the potential was derived by Hossain *et al.* [24,25] to analyze the ^{6}Li + ^{28}Si reaction at $E_{\rm Lab} = 7.5$–318.0 MeV, and was compared with WS and squared WS forms.

On the other hand, several studies have been carried out to investigate the single and double folding cluster (SFC and DFC) potentials based upon the α-cluster structure of the interacting nuclei in the analyses of α-nucleus and nucleus-nucleus elastic scattering, respectively [26–28]. In these studies, it was found that reducing the renormalization factor is essential to obtain a successful description of the scattering data. Abdullah and his collaborators [29–31], introduced a successful SFC approach to describe the elastic scattering differential cross sections of α particles on ^{12}C, ^{16}O, and ^{40,44,48}Ca targets as well as a DFC model for ^{16}O + ^{12}C scattering over a broad energy spectrum. No renormalization was required in their formalism to fit the data. Billah *et al.* [32] successfully used the same procedure to analyze the experimental differential cross-sections of α-elastic scattering on ^{58,60,62,64}Ni over a

wide range of incident energies. A reasonable description of the experimental data is thus obtained.

In the same way, Hassanain *et al.* [33] carried out two different versions of real cluster DF optical potential (DFC1 and DFC2) without renormalization factors, to reproduce successfully the $^{12}C + ^{12}C$ elastic-scattering data in the 70–360 MeV energy range. These researchers used the DFC1 potential and coupled-channels mechanism to successfully analyze the elastic and inelastic $^{12}C + ^{12}C$ scattering and $\alpha + ^{24}Mg$ (^{28}Si) elastic scattering in Refs. [34,35].

In the present paper, we have analyzed six sets of the $^{6}Li + ^{28}Si$ elastic-scattering data over the 76 to 318 MeV energy range by the use of the α-cluster folding formalism as an extension of our previous studies [36] for low energy. In the following section, we introduce the theoretical formalism for two different potential models, DFC1 and DFM. The latter was carried out by folding the M3Y-Paris effective *NN* interaction with finite range exchange (CDM3Y6). The calculation procedure is described in Sec. III. Section IV is devoted to results and discussion. Finally, conclusions are summarized in Sec. V.

II. THEORETICAL FORMALISM

In the present paper, we propose the α-cluster structure of the colliding nuclei to investigate elastic $^{6}Li + ^{28}Si$ scattering within the DFC1 model, considering the α-d cluster structure of ^{6}Li while the target $^{28}_{C}Si$ nucleus is considered as 7α particles. Thus, the real part of DFC1 is given by

$$V^{\mathrm{DFC1}}(R) = \int |\Psi(Z)|^2 \left[V_{\alpha-^{28}_{C}\mathrm{Si}}\left(\left|\vec{R} - \frac{1}{3}\vec{Z}\right|\right) + V_{d-^{28}_{C}\mathrm{Si}}\left(\left|\vec{R} + \frac{2}{3}\vec{Z}\right|\right)\right] dZ, \quad (1)$$

where R is the separation distance between the centers of projectile and target nuclei and Z is the α-d separation inside the ^{6}Li nucleus. The wave function of the relative motion of α and d clusters in the ground state of the ^{6}Li nucleus is $\Psi(Z)$ and is given by [36]

$$\Psi(Z) = N_0\, Z^2 \exp(-\gamma Z^2), \quad N_0 = \frac{4\gamma}{\sqrt{15}}\left(\frac{2\gamma}{\pi}\right)^{3/4}, \quad \gamma = 0.11\ \mathrm{fm}^{-2} \quad (2)$$

From this point of view we can formulate the $\alpha - ^{28}_{C}Si$ and $d - ^{28}_{C}Si$ interaction potentials as [36]

$$V_{\alpha-^{28}_{C}\mathrm{Si}}(r) = \int \rho_C(\acute{r}) V_{\alpha-\alpha}(|\vec{r} - \acute{\vec{r}}|) d\acute{\vec{r}} \quad (3)$$

and

$$\mathrm{V}_{d-^{28}_{C}\mathrm{Si}}(r) = \int \rho_C(\acute{r}) \mathrm{V}_{d-\alpha}(|\vec{r} - \acute{\vec{r}}|) d\acute{\vec{r}}\,, \quad (4)$$

TABLE I. Density parameters used in Eqs. (6) and (11) and corresponding $R_{\mathrm{rms.}}$.

Density distribution	ρ_0 (fm^{-3})	ω (fm^{-2})	C (fm)	β (fm)	A	$\langle r^2\rangle^{1/2}$ (fm)
$\rho_m(r)$	0.1775	−0.0142	3.2390	0.574	28	3.127
$\rho_C(r)$	0.0234	2.05374	3.0123	0.256	7	2.730

where

$$V_{d-\alpha}(r) = 2\int |\phi(Y)|^2 V_{n-\alpha}\left(\left|\vec{r} + \frac{1}{2}\vec{Y}\right|\right) d\vec{Y}. \quad (5)$$

Here $\rho_C(\acute{r})$ represents the full cluster density distribution of the ^{28}Si nucleus formed in the three-point Fermi (3pF) form [37] as

$$\rho_C(\acute{r}) = \rho_{0C}(1 + \omega\acute{r}^2)\left[1 + \exp\left(\frac{\acute{r} - C_\alpha}{\beta}\right)\right]^{-1}, \quad (6)$$

where ρ_{0C}, ω, C_α, and β parameters and the root mean square (rms) radius resulting from this form are shown in Table I.

Function $\phi(Y)$ is the s-state wave function of the proton-neutron relative motion inside the deuteron expressed as [36]

$$\phi(Y) = \left(\frac{2\lambda}{\pi}\right)^{3/4} e^{-\lambda Y^2}, \quad \lambda = 0.053\ \mathrm{fm}^{-2}, \quad (7)$$

where Y is the proton-neutron separation distance inside the deuteron. $V_{\alpha\text{-}\alpha}$ and $V_{n\text{-}\alpha}$ are effective interactions.

In our study, the phenomenological α-α effective interaction including a short-range repulsive and long-range attractive components was used with cluster approaches to avoid the traditional renormalization procedure in the folding cluster analysis. $\mathrm{V}_{\alpha\text{-}\alpha}$ [29–33] and $V_{n\text{-}\alpha}$ [33] are parametrized as

$$V_{\alpha\text{-}\alpha}(S) = V_R \exp\left(-\mu_R^2 S^2\right) - V_A \exp\left(-\mu_A^2 S^2\right), \quad (8)$$

$$V_{n\text{-}\alpha}(S) = -V_{0n} e^{-\chi S^2}, \quad (9)$$

where V_A and V_R respectively are the attractive and repulsive depths; μ_A and μ_R are the corresponding range parameters. We consider $V_A = 122.62$ MeV, $\mu_A = 0.469\ \mathrm{fm}^{-1}$ [38], and $\mu_R = 0.5\ \mathrm{fm}^{-1}$ [29], while the depth V_R is kept as a free parameter in the calculations. For the α-n effective interaction [36], $V_{0n} = 36.4$ MeV, and $\chi = 0.2657\ \mathrm{fm}^{-1}$.

To make a comparative study, the real microscopic folding approach built upon the CDM3Y6-Paris effective *NN* interaction is also carried out using computer code DFPD4 [39]. To generate this prescription, the nuclear matter densities distributions of the interacting nuclei with the density dependent M3Y finite range effective *NN* interaction are used. For more details see Refs. [40–42]. According to this approach, the matter density of ^{6}Li is taken as [43]

$$\rho_m^{^{6}\mathrm{Li}}(r) = 0.203\exp\left(-0.331 r_1^2\right) + \left(-0.0131 + 0.00138 r_1^2\right)\exp\left(-0.1584 r_1^2\right), \quad (10)$$

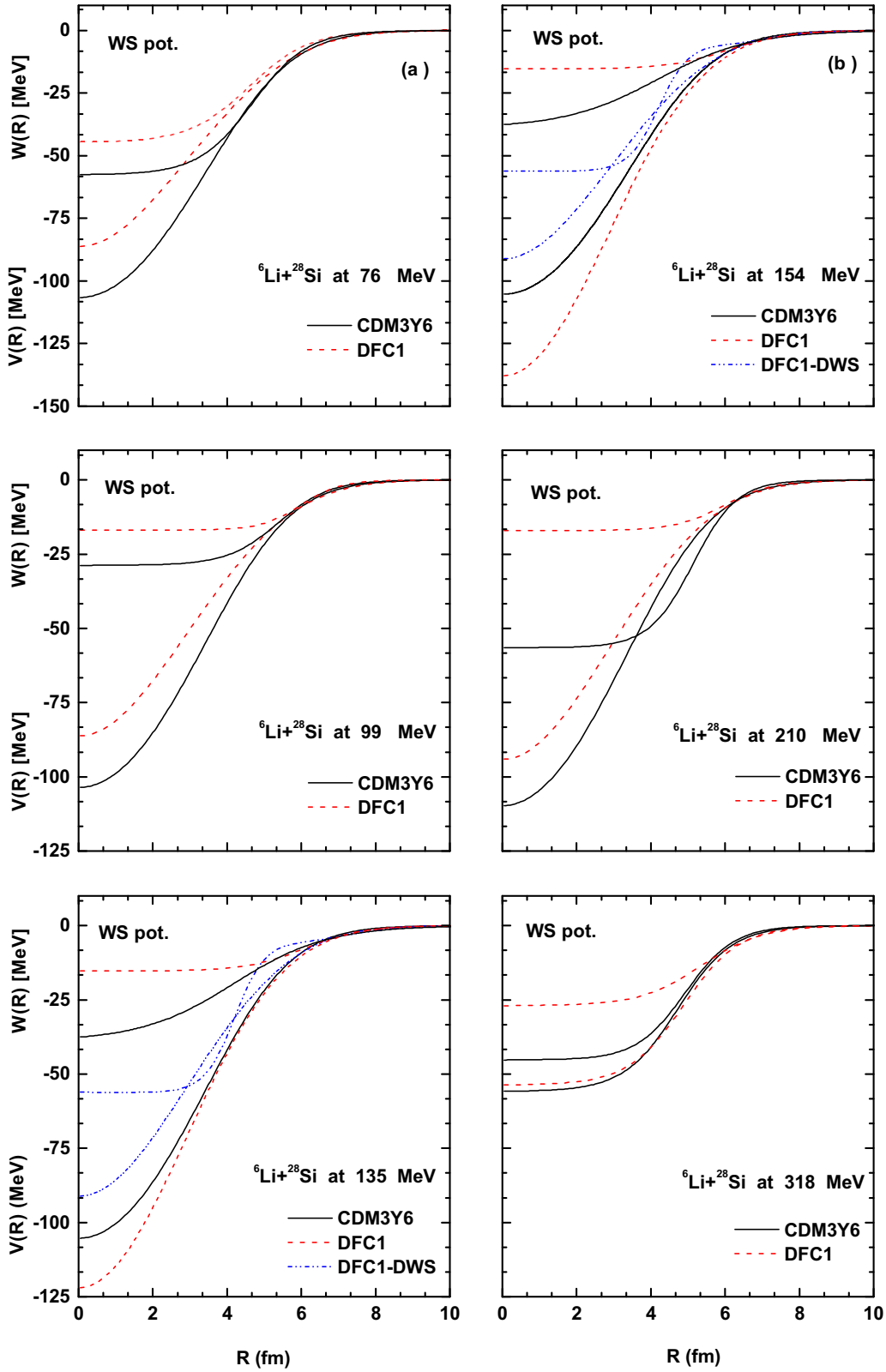

FIG. 1. A comparison of the radial shapes of the real microscopic nuclear potentials (DFC1 and CDM3Y6) and the WS imaginary potentials used in our calculations at $E_{\rm lab} = 76$–318 MeV. The dotted line is the real DFC1with (WS+DWS) imaginary potentials.

TABLE II. Best-fit parameters obtained from analyses of the elastic ^{6}Li + ^{28}Si scattering at $E_{\rm lab}$ = 76–318 MeV using semimicroscopic potentials. Values of parameter N_R for CDM3Y6 potentials are listed in the column labeled V_R.

Potential	V_R (MeV)	W_V (MeV)	r_V (fm)	a_V (fm)	W_D (MeV)	r_D (fm)	a_D (fm)	J_R (MeV fm^3)	J_R(MeV fm^3)	σ_R (mb)	χ^2
					$E_{\rm lab}$ = 76 MeV [49]						
DFC1	109.32	57.6	1.565	0.733				196.2	190.5	1629	9.4
CDM3Y6	0.5	44.71	1.533	0.81				199.74	145.79	1629	9.4
					$E_{\rm lab}$ = 99 MeV [13]						
DFC1	124.85	16.891	1.996	0.538				167.4	101.1	1522	33.2
CDM3Y6	0.43	28.77	1.795	0.689				179.0	134.5	1603	7.4
					$E_{\rm lab}$ = 135 MeV [2]						
DFC1	92.1	15.31	2.03	0.786				228.13	101.73	1807	31.3
DFC1-DWS	114.2	56.11	1.394	0.425	4.81	1.978	0.905	187.1	167.1	1952	12.2
CDM3Y6	0.56	38.89	1.397	1.25				222.13	138.10	2176	28.8
					$E_{\rm lab}$ = 154 MeV [13]						
DFC1	57.96	13.79	2.249	0.742				249.24	122.22	2027	14.9
DFC-DWS	113.3	56.81	1.338	0.372	7.13	1.702	1.060	188.8	184.4	1999	7.4
CDM3Y6	0.55	43.20	1.344	1.21				210.95	136.42	2037	20.0
					$E_{\rm lab}$ = 210 MeV [17]						
DFC1	73.85	17.06	1.992	0.665				261.99	105.4	1600	14.5
CDM3Y6	0.71	56.5	1.712	0.592				253.1	223.17	1499	10.0
					$E_{\rm lab}$ = 318 MeV [18]						
DFC1	56.81	27.01	1.784	0.826				293.6	131.56	1626	12.0
CDM3Y6	1.0	53.71	1.625	0.747				307.88	197.17	1565	14.2

while, the matter density of ^{28}Si is shown as follows [37]:

$$\rho_m^{^{28}\rm Si}(r) = \rho_{0m}(1.0 + \omega_m r^2)\left[1.0 + \exp\left(\frac{r - C_m}{\beta_m}\right)\right]^{-1}, \quad (11)$$

where ρ_{0m},ω_m, C_m, β_m, and $R_{\rm rms}$ parameters together with the corresponding rms radius are listed in Table I.

III. PROCEDURE

The microscopic DFC1and CDM3Y6 approaches generate the real part of the ^{6}Li − ^{28}Si optical potential while the imaginary part is taken as the volume WS potential. Thus, the total nuclear ^{6}Li + ^{28}Si potential is given by

$$U(r) = V_C(r) + U_{\rm DFC1(CDM3Y6)} - i W_V f_V(r), \quad (12)$$

where

$$f_V(r) = \left[1 + \exp\left(\frac{r - r_V\left(A_P^{1/3} + A_T^{1/3}\right)}{a_V}\right)\right]^{-1}. \quad (13)$$

The Coulomb potential $V_c(r)$ in our analysis was taken to be that of a uniform charged sphere of radius R_C = $1.4(6^{1/3} + 28^{1/3})$ fm. All considered real potentials given by the DFPD4 computer code [39] and our computer code [44] are fed into HI-OPTIM-94 [45]. The fits were obtained through the automatic search option in the program HI-OPTIM-94. The usual χ^2 criterion was used to judge the quality of agreement with the experimental data:

$$\chi^2 = \frac{1}{N_D}\sum_{k=1}^{N_D}\left[\frac{\sigma_{th}(\theta_k) - \sigma_{\rm exp}(\theta_k)}{\Delta\sigma(\theta_i)}\right]^2, \quad (14)$$

where $\sigma_{th}(\theta_k)$, $\sigma_{\rm exp}(\theta_k)$, and $\Delta\sigma(\theta_i)$ are the theoretical cross sections, the experimental cross sections, and the uncertainties in the experimental cross section, respectively. N_D is the number of data points for a given incident energy. An average value of 10% is used for the experimental errors of all considered data. The automatic searches were carried out by optimizing four (seven) free parameters: the depth of the real repulsive part of α-α interaction, V_R or the renormalization factor N_R for the CDM3Y6 interaction, plus another three (six) parameters of the imaginary phenomenological volume (volume + surface) WS potential. The experimental data were fit by minimizing the χ^2 parameter.

IV. RESULTS AND DISCUSSION

All potentials used in our calculations at the considered energies are shown in Fig. 1. We observe from this figure that the amplitudes of most of the real potentials are quite different at short internuclear distances, which correspond to the higher overlap density of the colliding nuclei, These large differences are not observed at radii in the surface region $R \sim$ 6.3 fm, which corresponds to the small overlap or low-density region. It is clearly seen that the DFC1 potential is shallower than the CDM3Y6 potential at short and medium distances, which leads to different descriptions of the large angle data for most energies. From Fig. 1, we see that the WS imaginary potentials for the microscopic CDM3Y6 potential are deeper than the DFC1potential for most of the energies studied here. Figure 1 shows also that the rms radius $\langle r^2\rangle^{1/2}$ for the potentials of CDM3Y6 are larger than those of the DFC1 ones.

Angular distributions of ^{6}Li + ^{28}Si elastic scattering cross sections at a wide energy range of $E_{\rm lab}$ = 76 to 318 MeV were fitted using the constructed DFC1 and CDM3Y6 approaches.

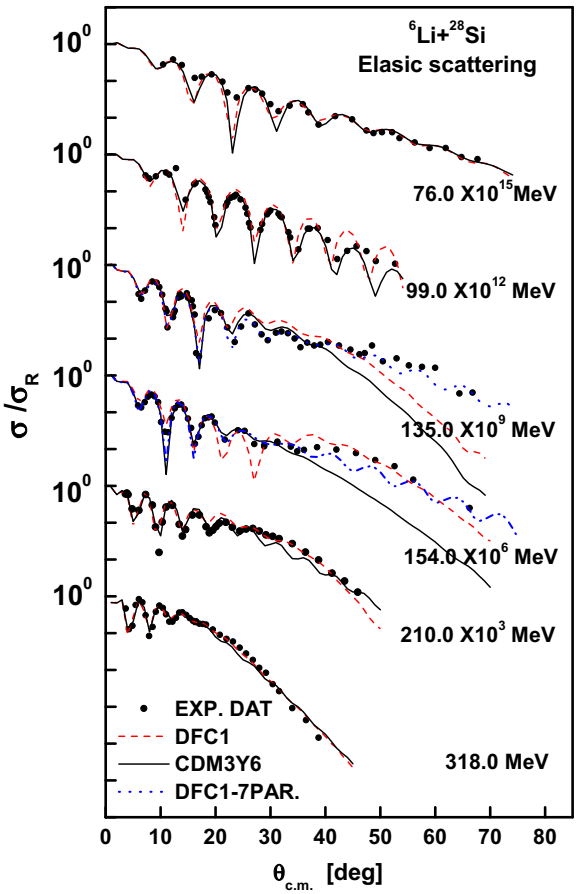

FIG. 2. A comparison between the measured ^{6}Li + ^{28}Si elastic differential cross sections and theoretical predictions obtained by using the CDM3Y6 and DFC1 potentials at $E_{\rm lab} = 76$, 99, 135, 154, 210, and 318 MeV. The dotted line is theoretical prediction using DFC1 with (WS+DWS) imaginary potentials. The data are taken from Refs. [13,17,18,49].

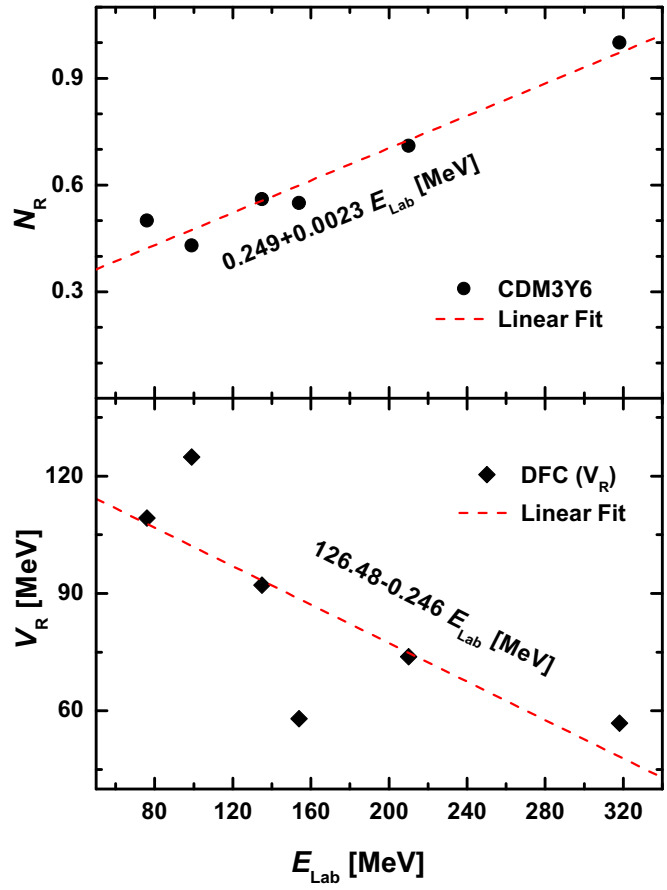

FIG. 3. Energy dependence of the best-fit parameters $N_{\rm R}$ and $V_{\rm R}$. Panels (a) and (b) show the results of energy dependence for the normalization coefficients ($N_{\rm R}$) of the CDM3Y6 potential and the real repulsive depths ($V_{\rm R}$) of the α-α interaction in the DFC1 potential, respectively.

Best fit parameters obtained for the real and imaginary potentials as well as the corresponding real and imaginary volume integrals per interacting nucleon pair J_R, J_I in MeV fm^3 and the reaction cross section σ_R in millibarns are reported in Table II. Figure 2 shows the calculation results in comparison with the experimental angular distributions of elastic ^{6}Li + ^{28}Si scattering at incident energies of $E_{\rm lab} = 76$, 99, 135, 154, 210, and 318 MeV. The solid and dashed curves show the results based upon CDM3Y6 and DFC1 potentials respectively. One may see that a satisfactory description of the data is achieved by using both considered potentials over most angular ranges, except there is a clear discrepancy in the backward angular region for two energies, 135 and 154 MeV, where the CDM3Y6 fits fall below the data at both energies and the DFC1 results fall below the data at 135 MeV. At the same time, both folded potentials give the same description of the data at higher, 318 MeV, and lower, 76 MeV, energies. This is shown in Fig. 2 that, due to the DFC1 potential being shallower than CDM3Y6 potential, the former results are overestimating that of CDM3Y6 for all energies, especially at backward angles. No renormalization factor was required for the DFC1 potentials to fit the data. Table II shows the χ^2 values for CDM3Y6 and DFC1 approaches for all considered energies. It is found that the values of χ^2 are similar for both potentials at all energies except at 99 MeV where significant change has been observed.

The weak binding of ^{6}Li makes it more susceptible to breakup in the field of the ^{28}Si target nucleus. For this purpose, the DPP which represents the effect of the coupling to breakup channels is added to the optical model calculations in an attempt to decrease the discrepancy with experimental data seen at 135 and 154 MeV [7–9]. Therefore, derivative (surface) WS potential (DWS) is combined with the volume WS imaginary potential for the energies (135 and 154 MeV). The DWS term is formed as [39]

$$W_D(r) = -4W_D \exp\left[r - r_D\left(A_P^{\frac{1}{3}} + A_T^{\frac{1}{3}}\right)/a_D\right]/ \left\{1 + \exp\left[r - r_D\left(A_P^{\frac{1}{3}} + A_T^{\frac{1}{3}}\right)/a_D\right]\right\}^2, \quad (15)$$

The automatic searches here were carried out by optimizing the obvious four free parameters indicated above plus the other three parameters of the imaginary phenomenological surface WS potential. The resulting potentials are shown in Fig. 1

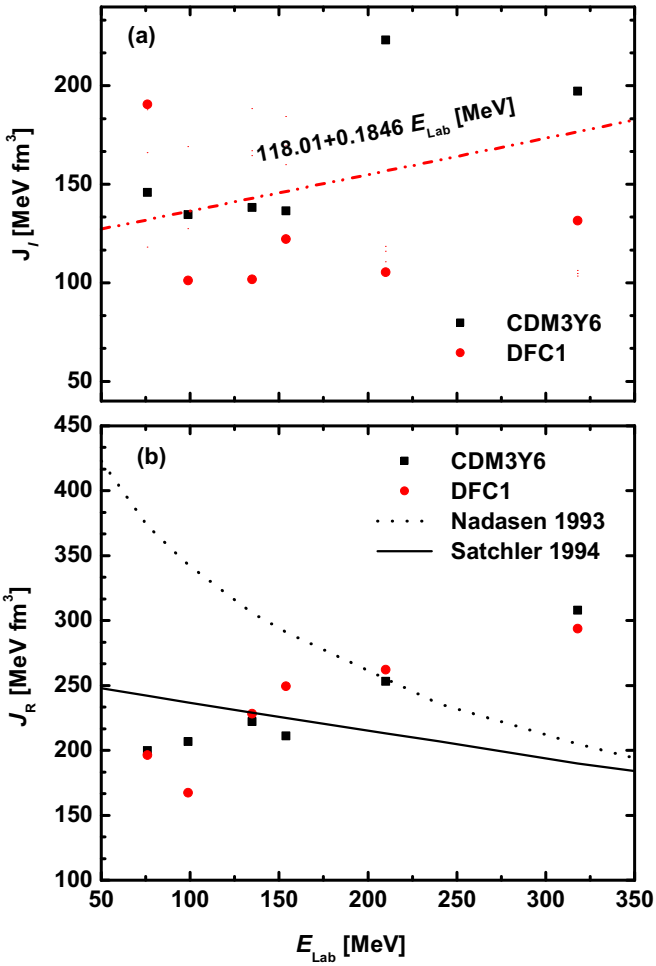

FIG. 4. The volume integral per interacting nucleon pair for different optical potentials of the ^{6}Li + ^{28}Si interaction obtained with CDM3Y6 and DFC1 and imaginary WS potentials plotted versus incident energy. The solid curve represents the Satchler expression obtained with the SIY effective *NN* interaction [48]. The dotted curve represents Nadisen *et al.*'s expression obtained with WS potentials [18].

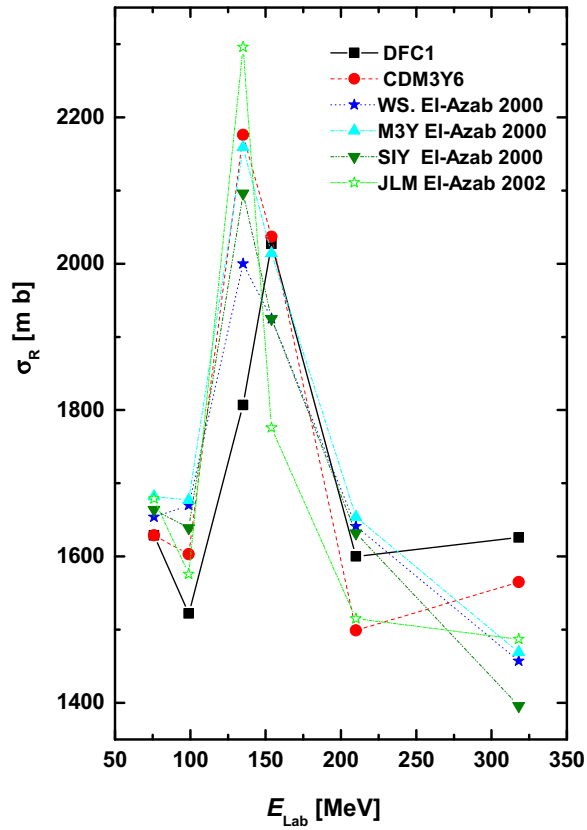

FIG. 5. Energy dependence of the total reaction cross sections, σ_R, extracted from the present analysis using CDM3Y6 and DFC1 potentials in comparison with those deduced from elastic scattering calculations of El-Azab [3,4].

as dotted lines. Improved agreement with experimental data especially at large angles is obtained as shown by the dotted curves in Fig. 2. This agrees with those results reported in Refs. [46,47]. The values of the DWS parameters are listed in Table II.

Figure 3 shows the best-fit parameters N_R and V_R (Table II) as a function of bombarding energy. The figure clearly indicates that the N_R factor for CDM3Y6 reveals a linearly increasing energy dependence as shown in Fig. 3(a). We notice from Table II that the renormalization factor N_R is still required for CDM3Y6 interaction in the range 0.43–0.56, to fit the data at low energies. In Fig. 3(b), the energy dependence of the real repulsive depth of α-α effective interaction V_R is shown. We notice that V_R reveals a negative linear energy dependence for all energies with simple diffraction at 99 and 135 MeV. We find $V_R = C - DE$, where $C = 126.48$ MeV, and $D = 0.246$ for the cluster approach. Figure 3 shows that as energy increases the values N_R increases, which corresponds to the decrease in the repulsive component in V_R.

The volume integrals per interacting pair of the real J_R and the imaginary J_I parts of the optical potential obtained from different models are listed in Table II. It is clear from Table II that the values of the real volume integrals given by the CDM3Y6 and DFC1 potentials are approximately the same over all the investigated energy range. These results are shown and compared to Satchler [48] and Nadasen *et al.*'s expressions [18] in Fig. 4(a). Satchler's expression is based on the folding model analysis of HI elastic scattering with the density dependent SIY effective *NN* interaction. Nadasen *et al.*'s formula is based on thephenomenological WS potential obtained from ^{6}Li elastic scattering on ^{28}Si, ^{40}Ca, and ^{90}Zr at 210 MeV. We notice that the values of the real volume integrals J_R obtained with CDM3Y6 and DFC1 approaches are in satisfactory agreement with Satchler's prediction below the 250 MeV energy range. This agreement is not found for Nadasen *et al.*'s prediction except at $E_{\rm lab} = 210$ MeV. By comparing our results with those performed by previous studies, we find that the CDM3Y6 results are consistent with those found by the phenomenological WS and DF potentials built upon M3Y, SIY, JLM, KH, and M3Y(R) in our previous study [3,4] in most considered energies. On the other side, we notice that our results are smaller than those obtained by the

DF potentials built upon M3Y-FR, M3Y-ZR, and JLM(R) [49] at several energies. The values of the imaginary volume integral J_I potentials obtained from the imaginary potentials supplemented with the two models' potentials are shown in Fig. 4(b).We also notice that the values of J_I seem to agree with our previous OM analysis of these data [3].

The calculated total reaction cross sections σ_R for ^{6}Li + ^{28}Si elastic scattering at all considered energies are reported in Table II. From Table II we notice that the values of σ_R obtained from both approaches have the same behavior. One see that the calculated values of σ_R from the present analysis by DFC1 are consistent with those obtained by using CDM3Y6 potentials, except at $E_{\rm lab} = 135$ MeV. Comparing our values for σ_R with those obtained by our previous studies, we find that the obtained σ_R are consistent with those obtained by using phenomenological WS and microscopic DF potentials based upon the M3Y, SIY, JLM, and KH approaches by Farid *et al.* [3,4]. To clarify this consistency, we plot the σ_R values extracted for the ^{6}Li + ^{28}Si system from the present analysis using the DFC1 and CDM3Y6 potentials versus energy in comparison with the previous studies [3,4] as shown in Fig. 5. Our results at the same energies are consistent with those obtained by Carstoiu *et al.* [49].

V. CONCLUSION

In the present study, we have shown a successful description of six sets of elastic scattering of the ^{6}Li + ^{28}Si interaction at bombarding energies ranging from 76 to 318 MeV by using two different versions of the real folding optical potential. In the first one, the full α cluster structure of the colliding nuclei is considered, where the ^{6}Li is described in terms of a d-α cluster-model wave function while the target nucleus ^{28}Si is described as 7α. Then the folded potential is generated for the contribution of α-α and n-α effective interactions folded with the cluster density distribution for projectile and target. The phenomenological α-α effective interaction including a short-range repulsive component and long-range attractive component was used to mitigate the need to use a conventional renormalization procedure in the cluster analysis. The nuclear potential was constructed by a generated real potential part supplemented with a phenomenological WS term as imaginary potential.

The microscopic potential based upon the effective CDM3Y6 Paris *NN* interaction is constructed. Both potentials, DFC1 and CDM3Y6, provide a good agreement with experimental data for ^{6}Li + ^{28}Si elastic scattering at all considered energies, except at larger scattering angles for 135 and 154 MeV data as noted in Sec. IV. We can see that the quality of fit of the data increases as the energy increases. On the other side, for the microscopic CDM3Y6 folding model calculations, a renormalization factor $N_R \approx 0.43$–1.0 is required to fit the experimental data over all the investigated energy range.

It is well established now that in the case of a weakly bound ^{6}Li projectile the real folding potential needs a significant reduction to account for estimated breakup channel effects on the elastic scattering channel. Therefore, the DPP is needed to describe the angular range, especially at backward angles of the cross sections. A complex surface potential, with a repulsive real part, is expected to simulate the breakup effect generated by the DPP. In the present study, we see that the repulsive component included in the phenomenological α-α effective interaction represents the repulsive real part of the DPP. On the other hand, the attractive imaginary DPP part is either included in the volume WS parameters or explicitly added to the volume WS potential as a derivative WS surface form. The former method was successful at all energies except for the obvious two energies 135 and 154 MeV, where the latter method was in better agreement with the data. It should be mentioned that including DPP effects in the CDM3Y6 model is beyond the scope of the present work.

The values of the real volume integrals obtained from both models are below Nadasen *et al.*'s predictions obtained with the WS potential model except at highest energy, but agree with Satchler's predictions obtained with the S1Y effective interaction, especially at low energies. At the same time, the imaginary volume integrals according to DFC1 calculations seem to be independent of the bombarding energy, and their values are in the range $J_I \approx 101$–190 MeV fm^3. The extracted total reaction cross sections are quite consistent with our previous studies but somewhat larger than those obtained by Carstoiu *et al.* Including the repulsive term in the phenomenological $\alpha\alpha$ effective interaction is not enough to fit the data, especially at backward angles in all cases. Therefore, we notice that the inclusion of the derivative surface DWS term in the imaginary potential is necessary for energies (e.g. 135 and 154 MeV) for this system, which describe the data at large angles.

Finally, from Ref. [36] and this current study, we confirm that the full cluster potential DFC1 has a powerful ability to reproduce successful descriptions of ^{6}Li + ^{28}Si elastic scattering data at low and high energies.

ACKNOWLEDGMENT

The first author extends appreciation to the Deanship of Scientific Research at King Khalid University for funding this work through the research groups program under Grant No. R.G.P.1/6/38.

[1] G. R. Satchler and W. G. Love, Phys. Rep. **55**, 183 (1979).
[2] R. M. DeVries, D. A. Goldberg, J. W. Watson, M. S. Zisman, and J. G. Cramer, Phys. Rev. Lett. **39**, 450 (1977).
[3] M. El-Azab Farid and M. A. Hassanain, Nucl. Phys. A **678**, 39 (2000).
[4] M. El-Azab Farid and M. A. Hassanain, Nucl. Phys. A **697**, 183 (2002).
[5] F. Carstoiu, L. Trache, R. E. Tribble, and C. A. Gagliardi, Phys. Rev. C **70**, 054610 (2004).
[6] M. E. Branden and G. R. Satchler, Phys. Rep. **285**, 143 (1997).
[7] Y. Sakuragi, M. Yahiro, and M. Kamimura, Prog. Theor. Phys. Suppl. **89**, 136 (1986).
[8] Y. Sakuragi, Phys. Rev. C **35**, 2161 (1987).

[9] Y. Sakuragi, M. Ito, Y. Hirabayashi, and C. Samanta, Prog. Theor. Phys. **98**, 521 (1997).
[10] H. G. Bingham, M. L. Halbert, D. C. Hensley, E. Newman, K. W. Kemper, and L. A. Charlton, Phys. Rev. C **11**, 1913 (1975).
[11] J. E. Poling, E. Norbeck, and R. R. Carlson, Phys. Rev. C **13**, 648 (1976).
[12] L. T. Chua, F. D. Becchetti, J. Jnecke, and F. L. Milder, Nucl. Phys. A **273**, 243 (1976).
[13] P. Schwandt, S. Kailas, W. W. Jacobs, M. D. Kaitchuck, W. Ploughe, and P. P. Singh, Phys. Rev. C **21**, 1656 (1980).
[14] S. Micek, Z. Majka, H. Rebel, H. J. Gils, and H. Klewe-Nebenius, Nucl. Phys. A **435**, 621 (1984).
[15] A. C. Demiyanova, V. N. Bragin, A. A. Ogloblin, A. L. Lebedev, J. M. Bang, S. A. Goncharov, S. N. Reshot, F. A. Gare, and P. P. Korovin, Phys. Lett. B **184**, 129 (1987).
[16] A. Nadasen, M. McMaster, G. Gunderson, A. Judd, S. Villanueva, P. Schwandt, J. S. Winfield, J. van der Plicht, R. E. Warner, F. D. Becchetti, and J. W. Janecke, Phys. Rev. C **37**, 132 (1988).
[17] A. Nadasen, M. McMaster, M. Fingal, J. Tavormina, P. Schwandt, J. S. Winfield, M. F. Mohar, F. D. Becchetti, J. W. Janecke, and R. E. Warner, Phys. Rev. C **39**, 536 (1989).
[18] A. Nadasen, T. Stevens, J. Farhat, J. Brusoe, P. Schwandt, J. S. Winfield, G. Yoo, N. Anantaraman, F. D. Becchetti, J. Brown, B. Hotz, J. W. Janecke, D. Roberts, and R. E. Warner, Phys. Rev. C **47**, 674 (1993).
[19] K. Schwarz, C. Samanta, M. Fujiwara, H. Rebel, R. De Leo, N. Matsuoka, H. Utsunomiya, H. Akimune, I. Daito, H. Fujimura, F. Ihara, K. Ishibashi1, Y. Maeda, T. Yamanaka, H. Yoshida, A. Okihana, T. Yoshimura, P. K. J. van Aarle, W. A. T. Uijen, M. Ito, and Y. Sakuragi, Eur. Phys. J. A **7**, 367 (2000).
[20] M. El-Azab Farid, K. O. Behairy, and Z. M. M. Mahmoud, Braz. J. Phys. **44**, 73 (2013).
[21] X. Chen, Y.-W. Lui, H. L. Clark, Y. Tokimoto, and D. H. Youngblood, Phys. Rev. C **80**, 014312 (2009).
[22] X. Chen, Y.-W. Lui, H. L. Clark, Y. Tokimoto, and D. H. Youngblood, Phys. Rev. C **76**, 054606 (2007).
[23] Krishichayan, X. Chen, Y.-W. Lui, J. Button, and D. H. Youngblood, Phys. Rev. C **81**, 044612 (2010).
[24] S. Hossain, M. N. A. Abdullah, A. S. B. Tariq, M. A. Uddin, A. K. Basak, K. M. Rusek, I. Reichstein, and F. B. Malik, Europhys. Lett. **84**, 52001 (2008).
[25] S. Hossain, M. N. A. Abdullah, A. K. Basak, S. K. Das, M. A. Uddin, A. S. B. Tariq, I. Reichstein, K. M. Rusek, and F. B. Malik, Eur. Phys. J. A **41**, 215 (2009).
[26] M. El-Azab Farid, Z. M. M. Mahmoud, and G. S. Hassan, Nucl. Phys. A **691**, 671 (2001); Phys. Rev. C **64**, 014310 (2001).
[27] M. El-Azab Farid, Phys. Rev. C **65**, 067303 (2002).
[28] M. Karakoc and I. Boztosun, Phys. Rev. C **73**, 047601 (2006); Int. J. Mod. Phys. E **15**, 1317 (2006).
[29] M. N. A. Abdullah, S. Hossain, M. S. I. Sarker, S. K. Das, A. S. B. Tariq, M. A. Uddin, A. K. Basak, S. Ali, H. M. Sen Gupta, and F. B. Malik, Eur. Phys. J. A **18**, 65 (2003).
[30] M. N. A. Abdullah, M. S. I. Sarker, S. Hossain, S. K. Das, A. S. B. Tariq, M. A. Uddin, A. S. Mondal, A. K. Basak, S. Ali, H. M. Sen Gupta, and F. B. Malik, Phys. Lett. B **571**, 45 (2003).
[31] S. Hossain, M. N. A. Abdullah, K. M. Hasan, M. Asaduzzaman, M. A. R. Akanda, S. K. Das, A. S. B. Tariq, M. A. Uddin, A. K. Basak, S. Ali, and F. B. Malik, Phys. Lett. B **636**, 248 (2006).
[32] M. M. Billah, M. N. A. Abdullah, S. K. Das, M. A. Uddin, A. K. Basak, I. Reichstein, H. M. Sen Gupta, and F. B. Malik, Nucl. Phys. A **762**, 50 (2005).
[33] M. A. Hassanain, A. A. Ibraheem, and M. El-Azab Farid, Phys. Rev. C **77**, 034601 (2008).
[34] M. A. Hassanain, Prog. Theor. Phys. **126**, 269 (2011).
[35] M. A. Hassanain, Int. J. Mod. Phys. E **20**, 1931 (2011).
[36] M. El-Azab Farid, Awad A. Ibraheem, J. H. Al-Zahrani, W. R. Al-Harbi, and M. A. Hassanain, J. Phys. G: Nucl. Part. Phys. **40**, 075108 (2013).
[37] H. de Vries, C. W. de Jager, and C. de Vries, At. Data Nucl. Data Tables **36**, 495 (1987).
[38] M. A. Hassanain, Awad A. Ibraheem, Shikha M. M. Al Sebiey, S. R. Mokhtar, M. A. Zaki, Zakaria M. M. Mahmoud, K. O. Behairy, and M. El-Azab Farid, Phys. Rev. C **87**, 064606 (2013).
[39] D. T. Khoa, computer program DFPD4 (private communication).
[40] D. T. Khoa, G. R. Satchler, and W. von Oertzen, Phys. Rev. C **51**, 2069 (1995).
[41] D. T. Khoa and W. von Oertzen, Phys. Lett. B **304**, 8 (1993).
[42] G. Bertsch, J. Borysowicz, H. McManus, and W. G. Love, Nucl. Phys. A **284**, 399 (1977).
[43] K. H. Bray, M. Jain, K. S. Jayaraman, G. Lobianco, G. A. Moss, W. T. H. Oers, D. O. Wells, and F. Petrovich, Nucl. Phys. A **189**, 35 (1972).
[44] M. A. Hassanain, M. Anwar, and K. O. Behairy (unpublished).
[45] N. M. Clarke, HI-OPTIM 94.2 Code (private communication) (1994).
[46] M. P. Nicoli, F. Haas, R. M. Freeman, S. Szilner, Z. Basrak, A. Morsad, G. R. Satchler, and M. E. Brandan, Phys. Rev. C **61**, 034609 (2000).
[47] M. A. Hassanain, Eur. Phys. J. A **52**, 8 (2016).
[48] G. R. Shatchler, Nucl. Phys. A **579**, 241 (1994).
[49] F. Carstoiu and M. Lassaut, Nucl. Phys. A **597**, 269 (1996).